



Supplement of

Interpreting the cause of bound earthquakes at underground injection experiments

Ryan Schultz et al.

Correspondence to: Ryan Schultz (ryan.schultz@sed.ethz.ch)

The copyright of individual parts of the supplement might differ from the article licence.

27 **Supplementary Text**

28

29 *S1: Stage drop-out test at PNR-1z*

30 Here, we perform a perturbation analysis to better understand how the EW-test responds
31 to poorly-resolved cases. To do so, we start with the PNR-1z dataset and perform the EW-test
32 using data from all the stages as a single cluster. We then omit the first stage from the cluster of
33 earthquakes and then perform the EW-test again. This drop-out process is sequentially repeated
34 until only the last stage is left. This perturbation is the same as those already presented in this
35 manuscript, and similar to those from prior studies (Schultz et al., 2025).

36 We plot a smoothed version of this analysis (Figure S16). This analysis indicates that the
37 best resolved cluster is (unsurprisingly) the one that includes all stage information, with a best-fit
38 n -exponent of ~ 1.6 . As initial stages sequentially drop-out, the confidence in the cluster being
39 bound generally decreases and the n -exponent also decreases. Eventually enough data is removed
40 such that we fall below the thresholds for statistical confidence and an n -exponent of 0.5 is
41 approached.

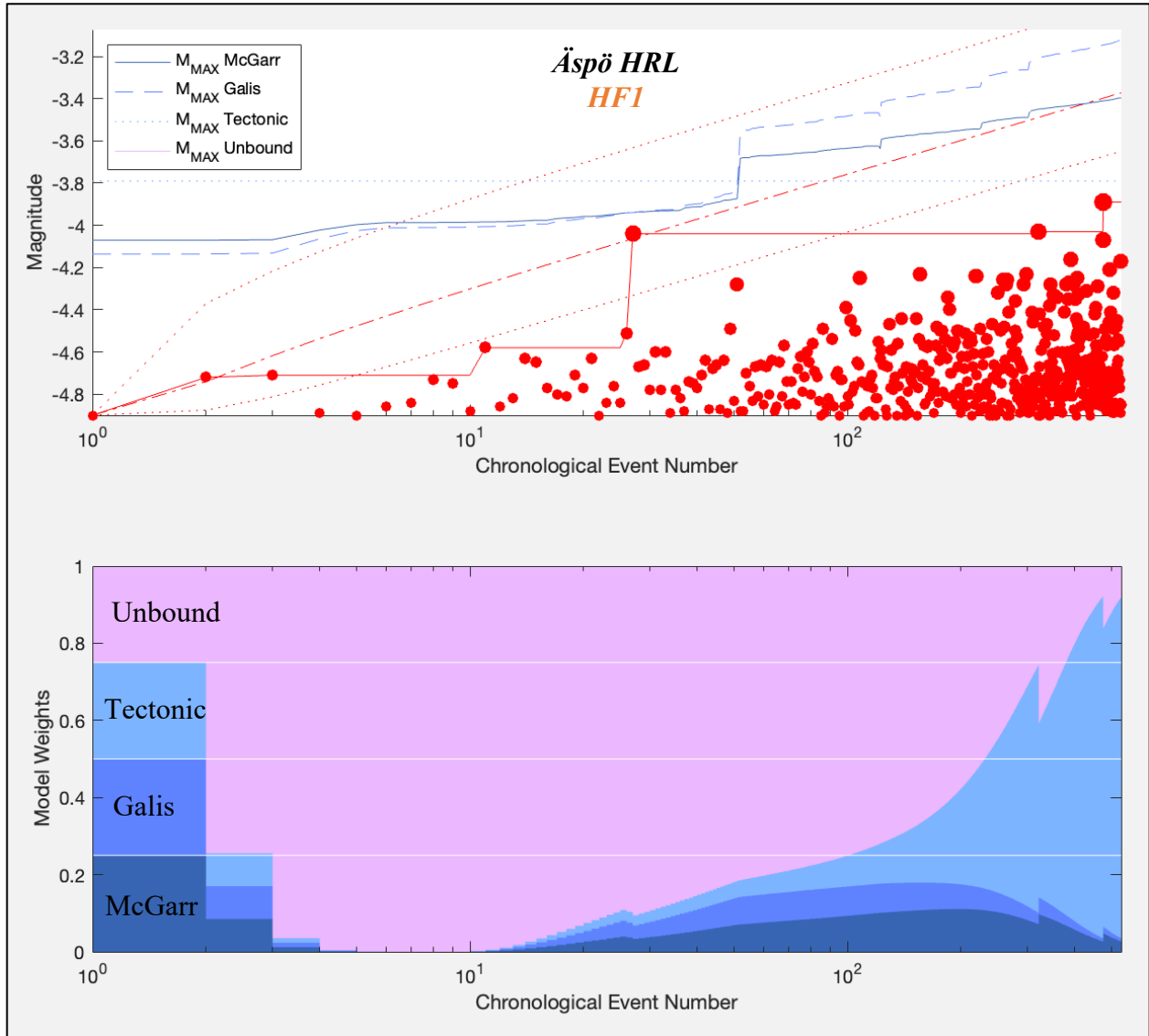
42 Generally, this observation supports our interpretation of bound-fractures and unbound-
43 faults (Figure 13). In this drop-out analysis, omitting earlier stages would be expected to
44 increasingly ignore the initial creation of the fracture network. In this sense, drop-out
45 progressively emulates stimulation into a large pre-existing fracture network. Thus, an unbound
46 response is expected in the limit of only considering the last stage – since there is already a large
47 and extensive pre-existing fracture network for M_{LRG} events to grow into uninhibited. If enough
48 drop-out stages are reincorporated back into the cluster, the response starts appearing tectonic-like
49 (or X-like), since the (apparent) unbound growth eventually encounters an abrupt upper limit (and
50 this limit is not well-resolved enough to sense its change with time). Next, an intermediate amount
51 of drop-out would encounter this abrupt upper limit, and start to sense its change with time, but
52 not well enough to accurately constrain the n -exponent. In the final limit, our data is well-resolved
53 enough to accurately constrain the true n -exponent.

54 This highlights the importance of capturing the initial M_{LRG} events for accurate EW-test
55 results for cases with volume-based M_{MAX} . Conversely, this also highlights a potential
56 observational bias within the EW-test, regarding the accuracy of the n -exponent. Because of this,
57 we favour the observational bias as the most likely explanation of the X-like n -exponent (Figure

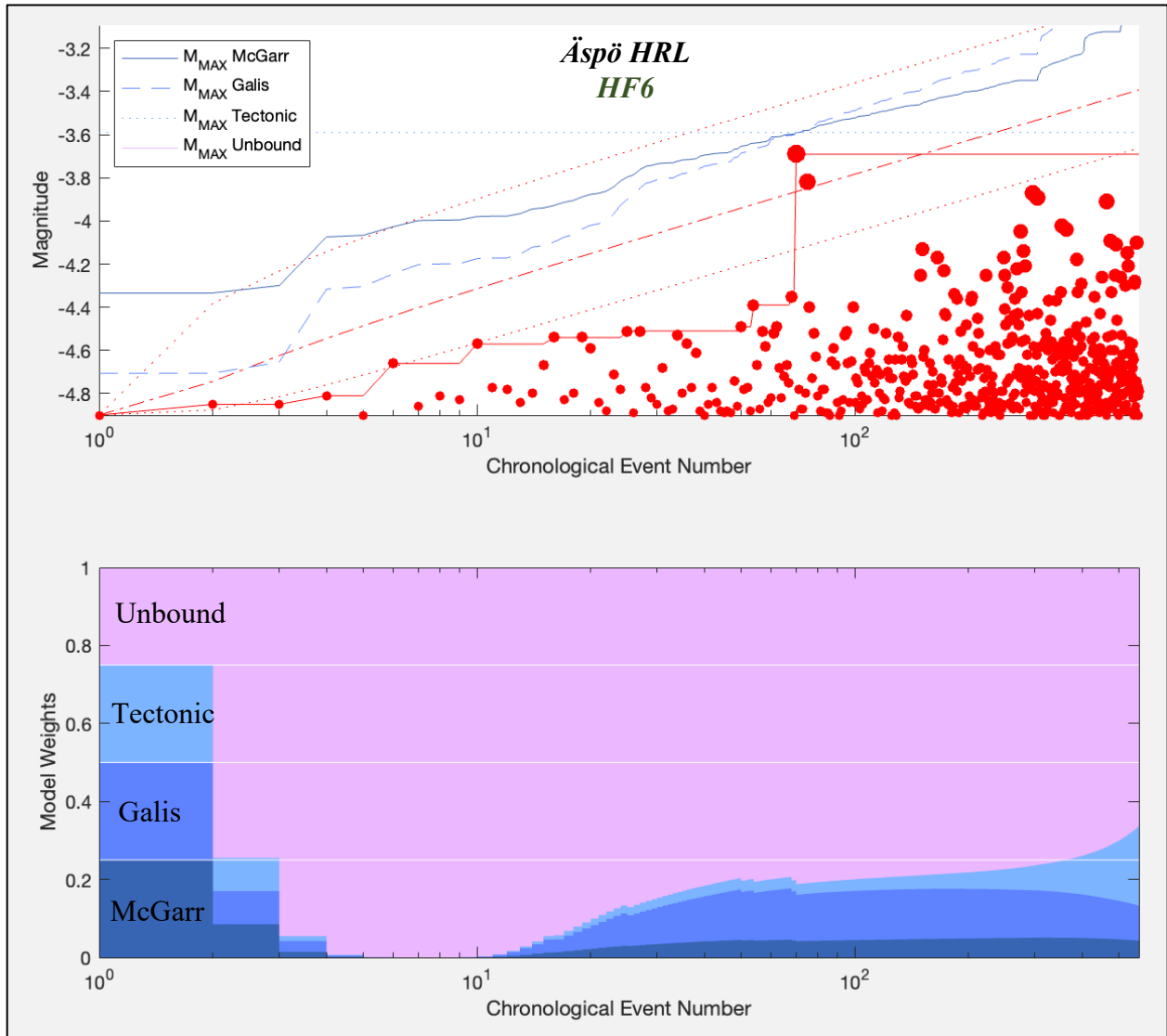
58 15). We note that this observational bias will likely be relevant in realistic settings – such as for
59 hydraulic fracturing stimulations starting in a perforated well. Potentially, this bias could be
60 accounted for by including a y-intercept term to volume-based M_{MAX} relationships.

61

62 **Supplementary Figures**
63



64
65
66 **Figure S1. Using the EW-test to discern between M_{MAX} models for HF1 at the Äspö HRL.** In
67 the catalogue of earthquake magnitudes (red circles) and the observed M_{LRG}
68 sequence (red lines & circles), and expected M_{LRG} at the 10/50/90 percentiles (red dashed lines)
69 are tested using three M_{MAX} assumptions (blue lines). In the bottom panel, AIC/BIC-based
70 ensemble model weights (blue bars) using all data prior to each new M_{LRG} value are shown.
71
72



74

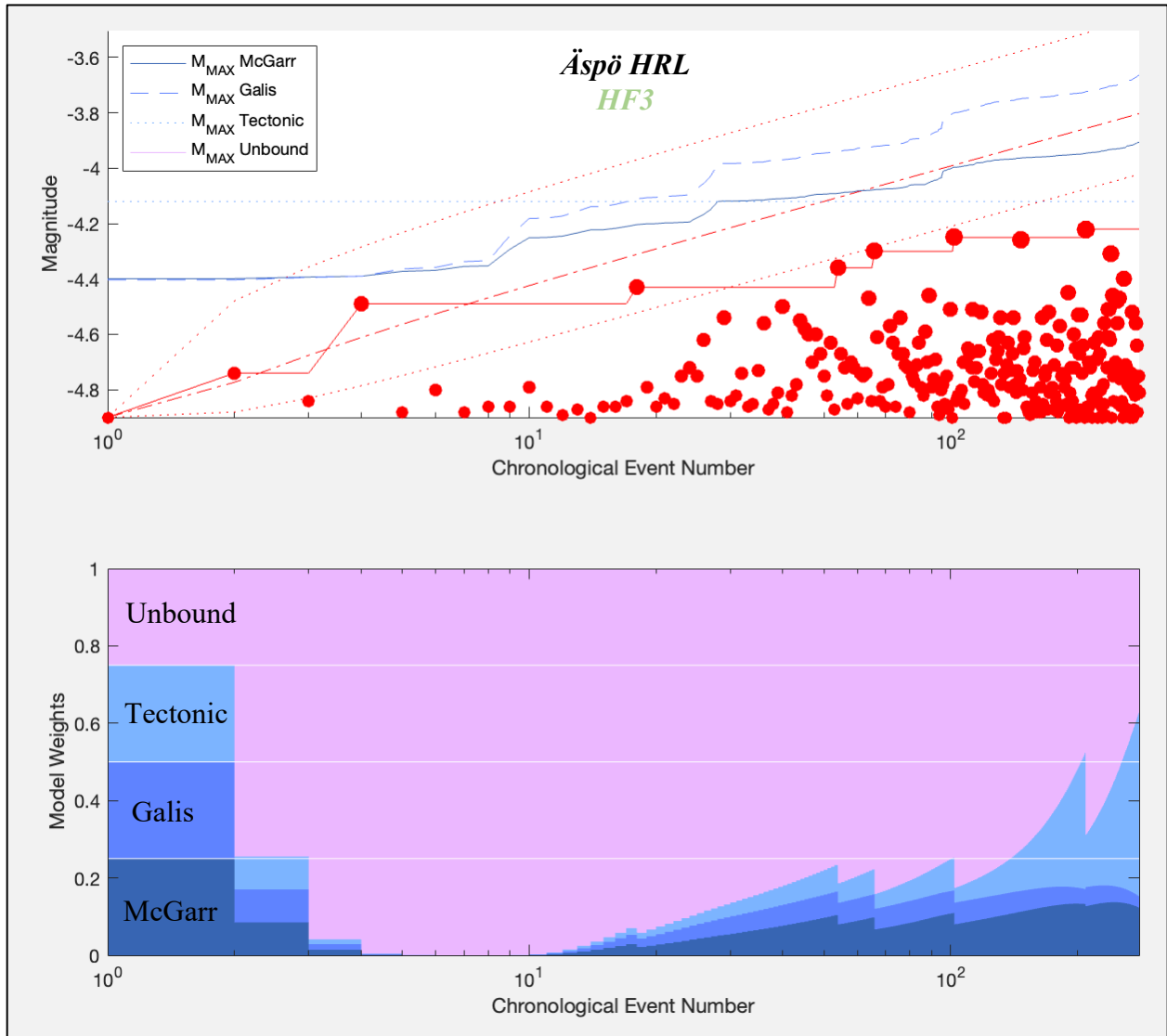
75

76 **Figure S2. Using the EW-test to discern between M_{MAX} models for HF6 at the Äspö HRL.**77 In the top panel, the catalogue of earthquake magnitudes (red circles), the observed M_{LRG} sequence78 (red lines & circles), and expected M_{LRG} at the 10/50/90 percentiles (red dashed lines) are tested79 using three M_{MAX} assumptions (blue lines). In the bottom panel, AIC/BIC-based ensemble model

80 weights (coloured bars) using all data prior to each new event are shown.

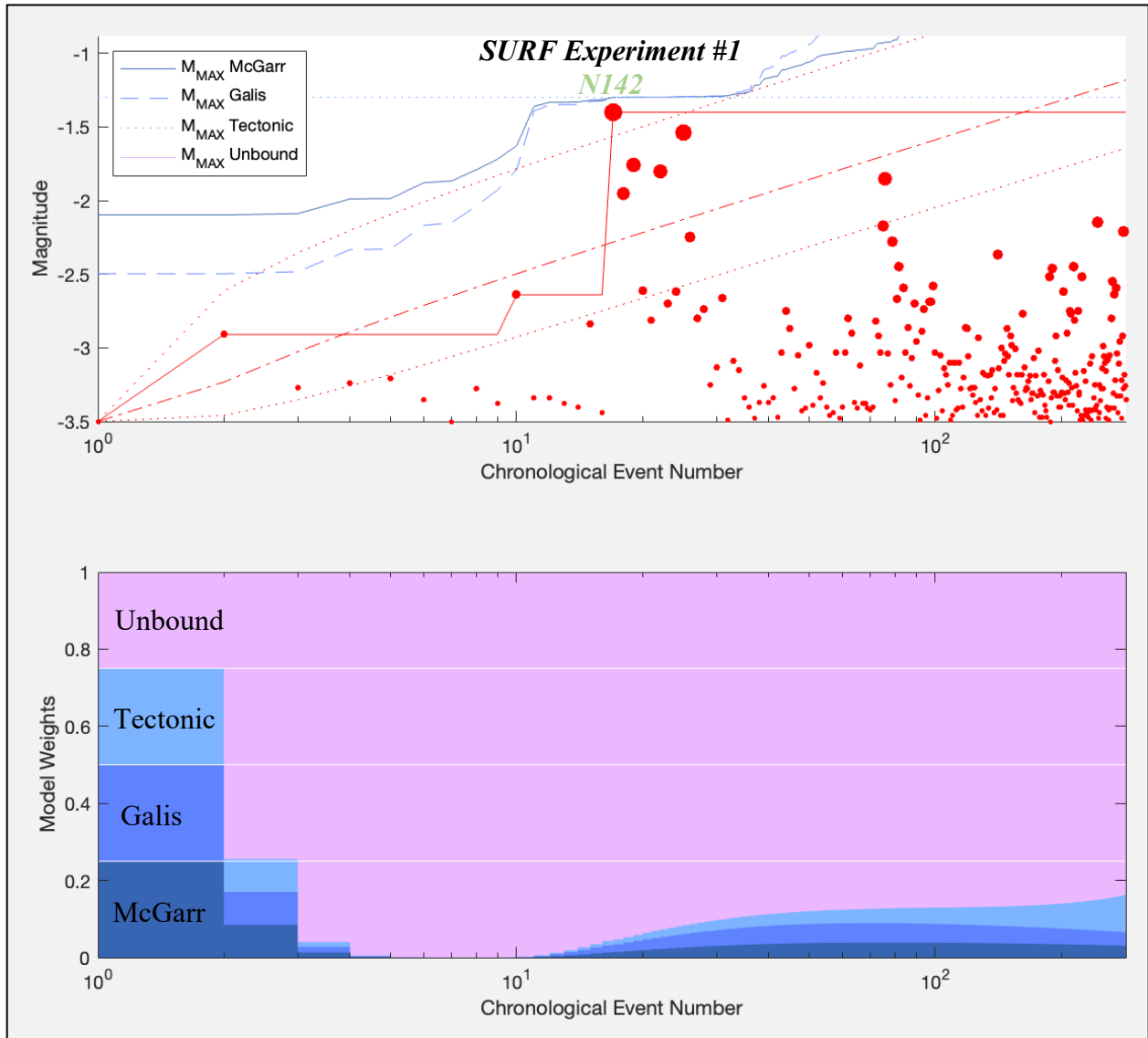
81

82



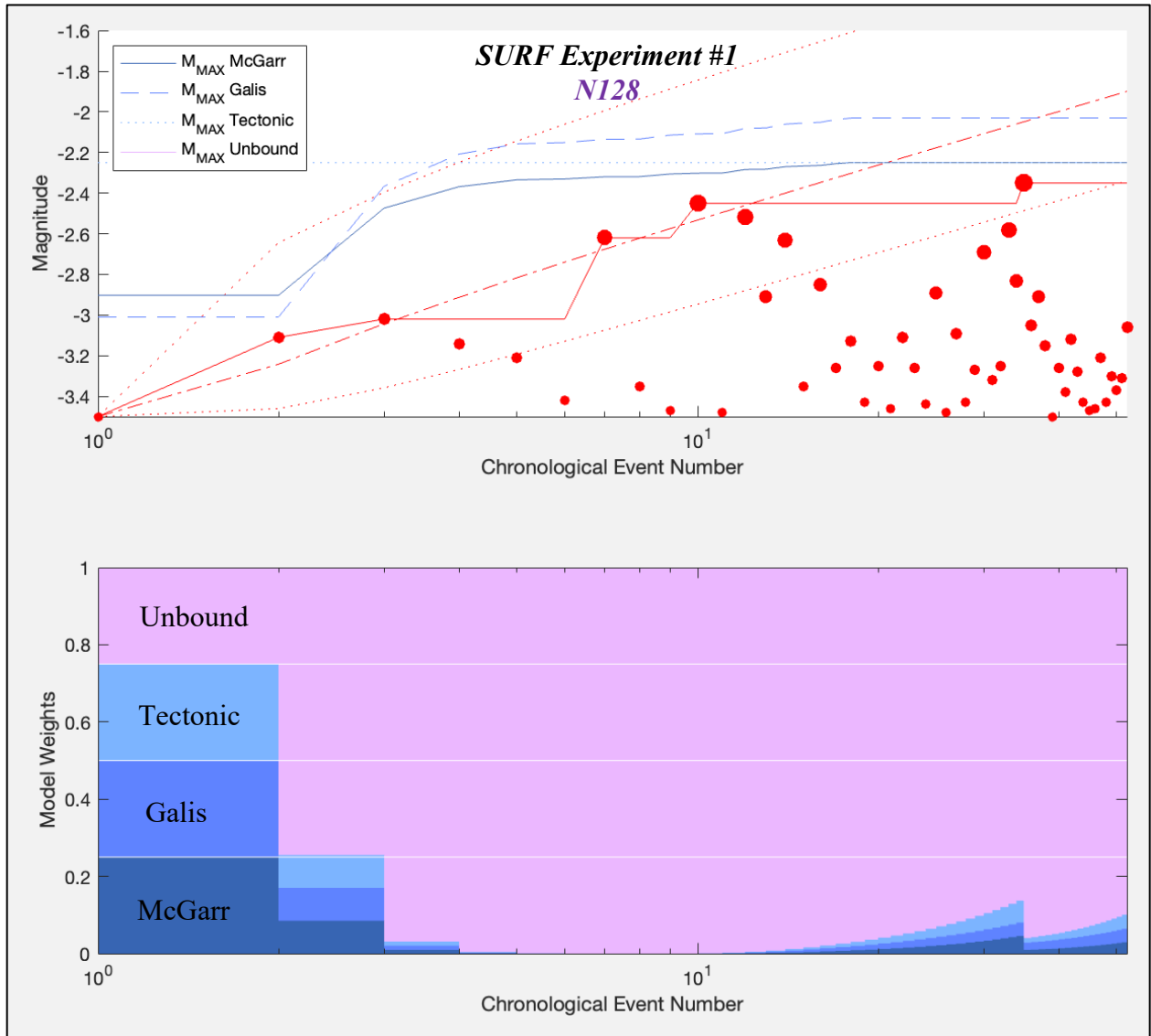
84
85
86
87
88
89
90
91
92

Figure S3. Using the EW-test to discern between M_{MAX} models for HF3 at the Äspö HRL. In the top panel, the catalogue of earthquake magnitudes (red circles), the observed M_{LRG} sequence (red lines & circles), and expected M_{LRG} at the 10/50/90 percentiles (red dashed lines) are tested using three M_{MAX} assumptions (blue lines). In the bottom panel, AIC/BIC-based ensemble model weights (coloured bars) using all data prior to each new event are shown.



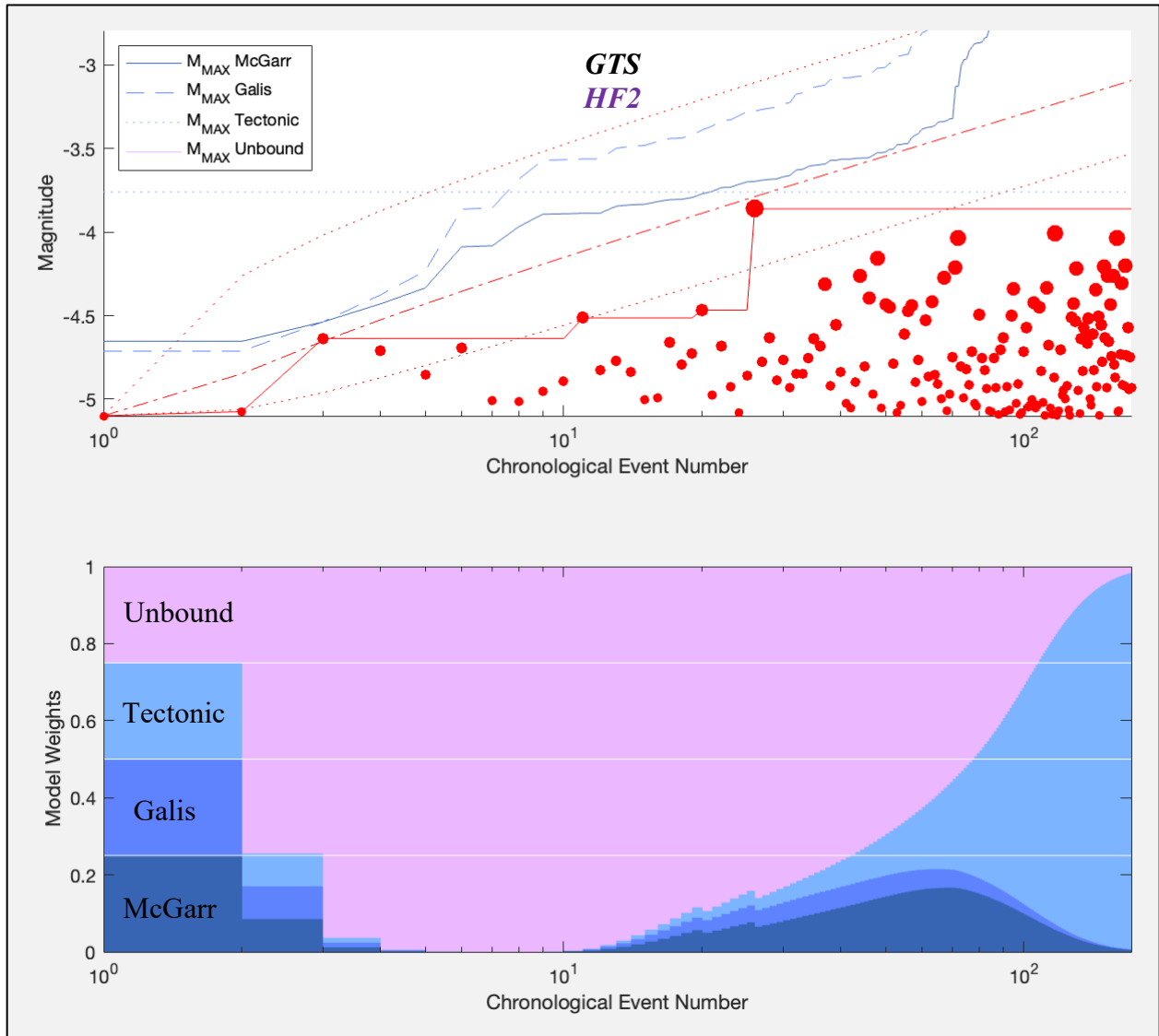
94
 95
 96
 97
 98
 99
 100
 101
 102

Figure S4. Using the EW-test to discern between M_{MAX} models for N142 at SURF Experiment #1. In the top panel, the catalogue of earthquake magnitudes (red circles), the observed M_{LRG} sequence (red lines & circles), and expected M_{LRG} at the 10/50/90 percentiles (red dashed lines) are tested using three M_{MAX} assumptions (blue lines). In the bottom panel, AIC/BIC-based ensemble model weights (coloured bars) using all data prior to each new event are shown.



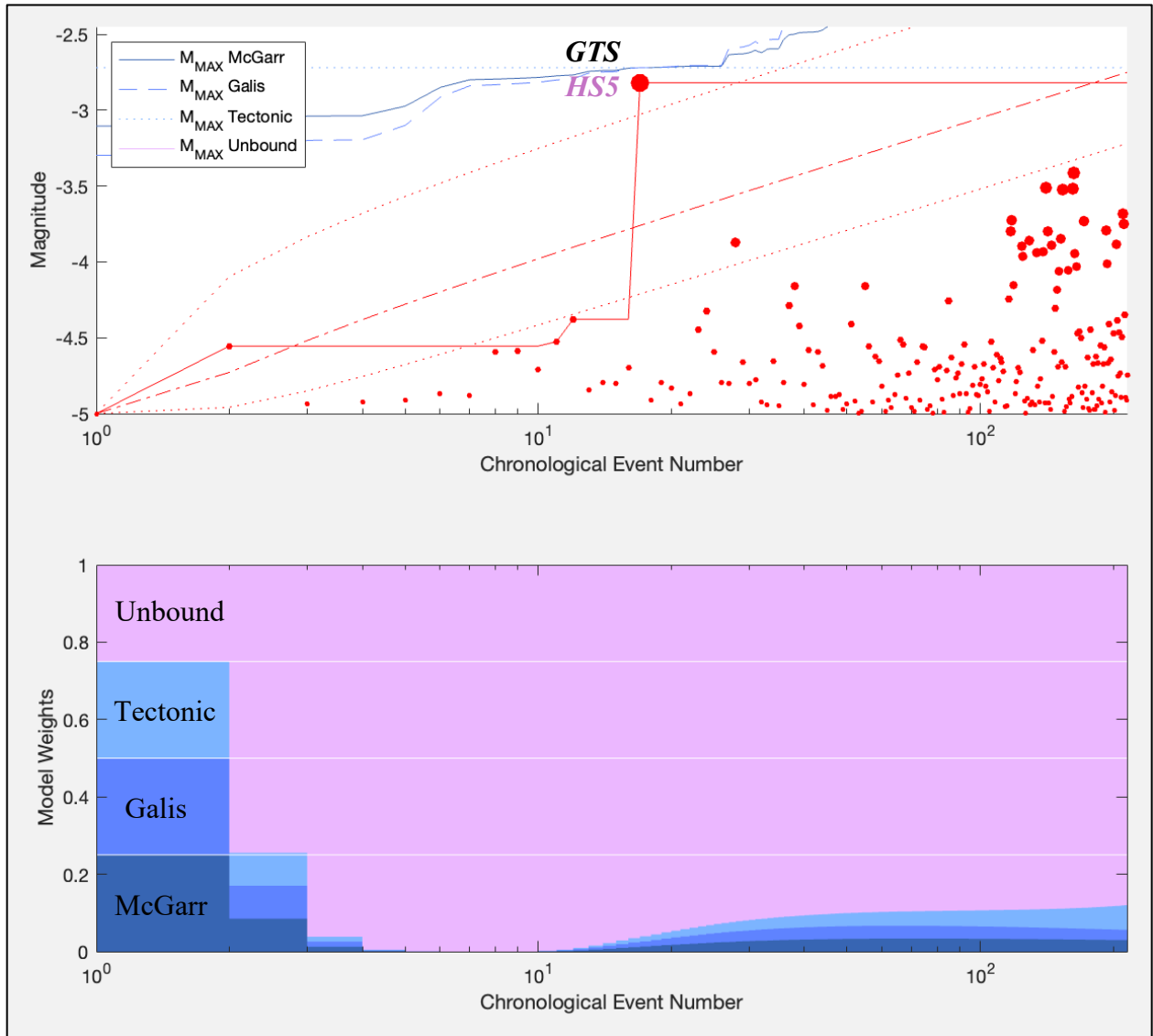
104
 105
 106
 107
 108
 109
 110
 111
 112

Figure S5. Using the EW-test to discern between M_{MAX} models for N128 at SURF Experiment #1. In the top panel, the catalogue of earthquake magnitudes (red circles), the observed M_{LRG} sequence (red lines & circles), and expected M_{LRG} at the 10/50/90 percentiles (red dashed lines) are tested using three M_{MAX} assumptions (blue lines). In the bottom panel, AIC/BIC-based ensemble model weights (coloured bars) using all data prior to each new event are shown.



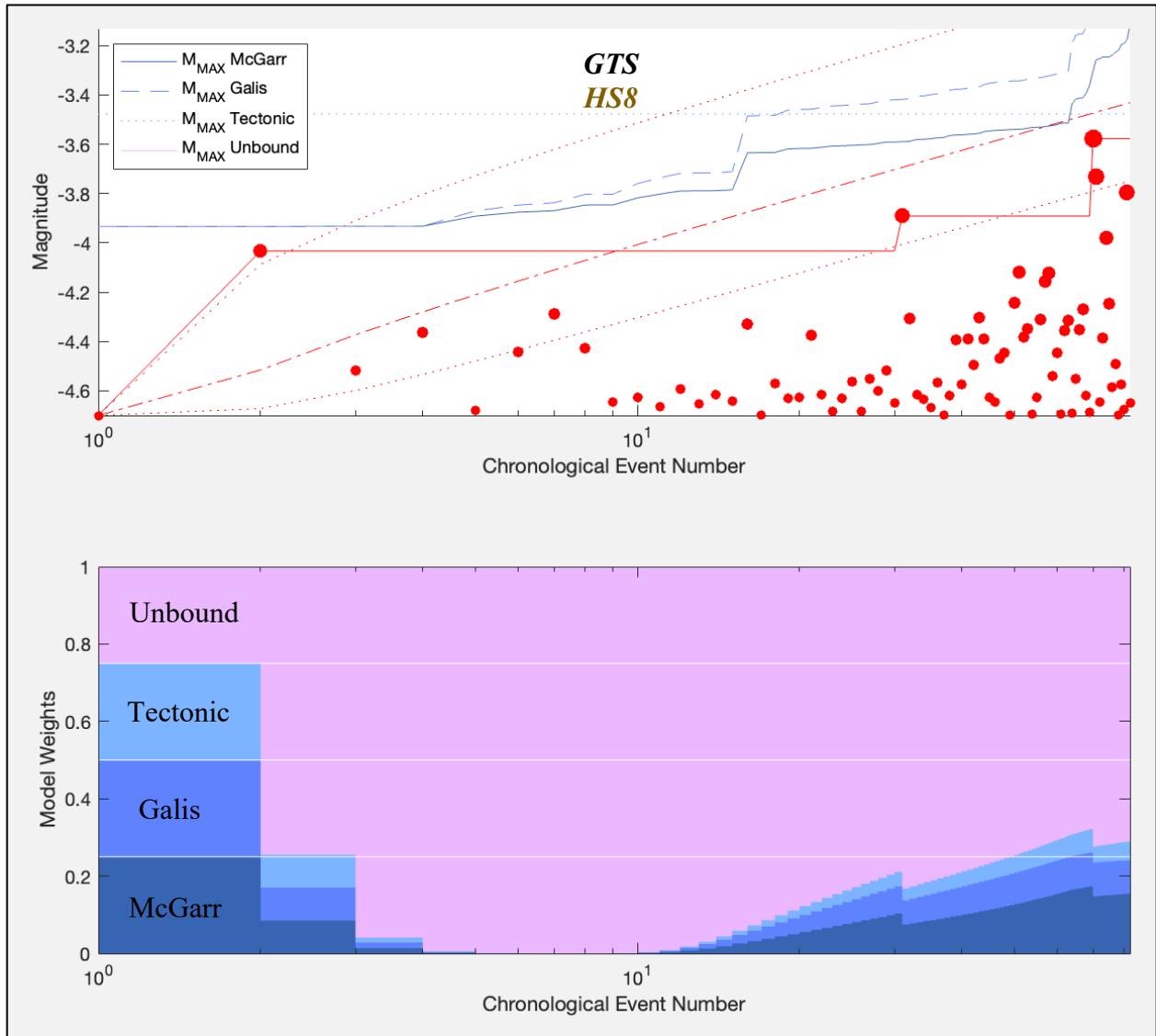
114
 115
 116
 117
 118
 119
 120
 121
 122

Figure S6. Using the EW-test to discern between M_{MAX} models for HF2 at the GTS. In the catalogue of earthquake magnitudes (red circles), the observed M_{LRG} sequence (red lines & circles), and expected M_{LRG} at the 10/50/90 percentiles (red dashed lines) are tested using three M_{MAX} assumptions (blue lines). In the bottom panel, AIC/BIC-based ensemble model weights (coloured bars) using all data prior to each new event are shown.



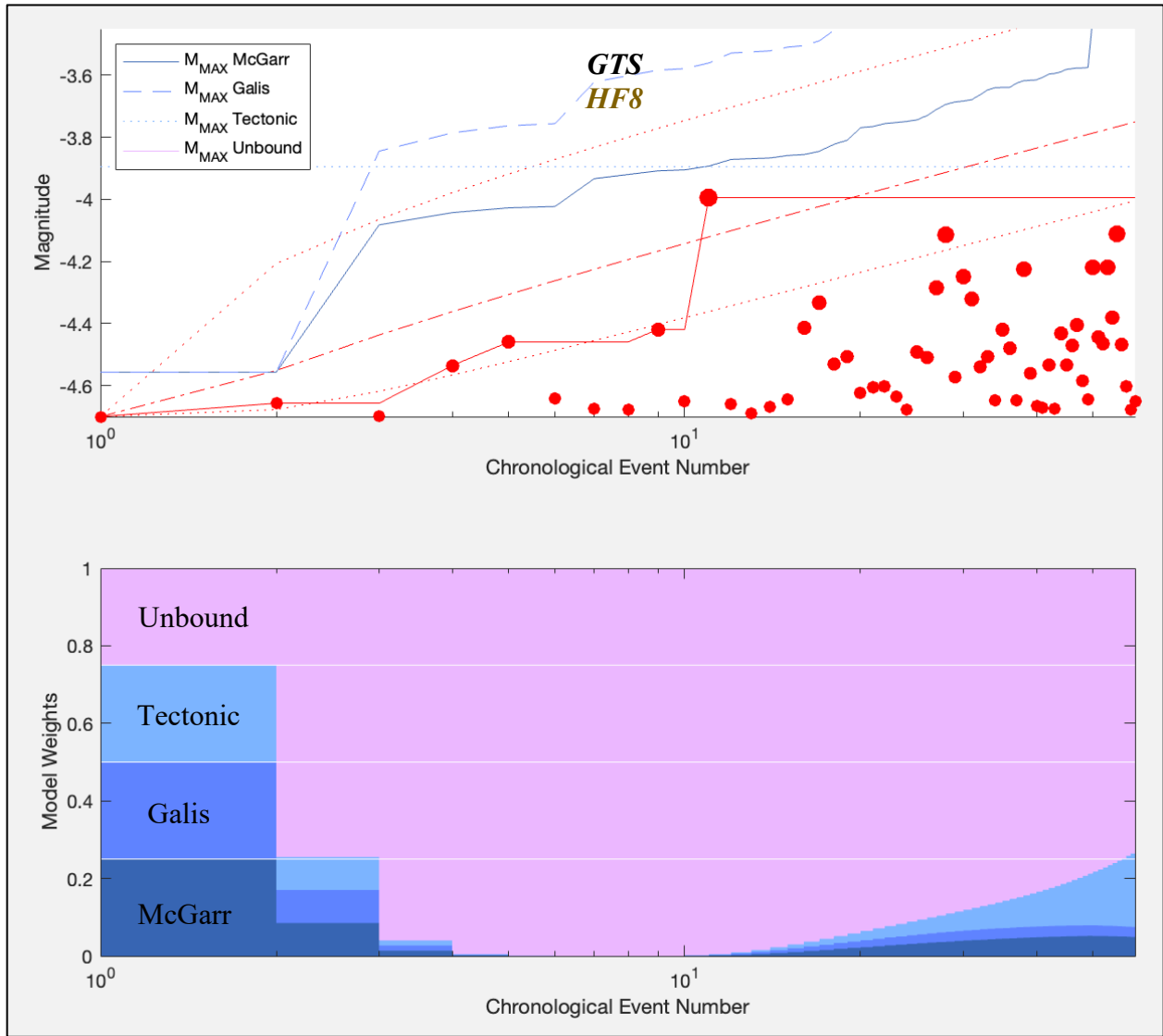
124
 125
 126
 127
 128
 129
 130
 131
 132

Figure S7. Using the EW-test to discern between M_{MAX} models for HS5 at the GTS. In the top panel, the catalogue of earthquake magnitudes (red circles), the observed M_{LRG} sequence (red lines & circles), and expected M_{LRG} at the 10/50/90 percentiles (red dashed lines) are tested using three M_{MAX} assumptions (blue lines). In the bottom panel, AIC/BIC-based ensemble model weights (coloured bars) using all data prior to each new event are shown.



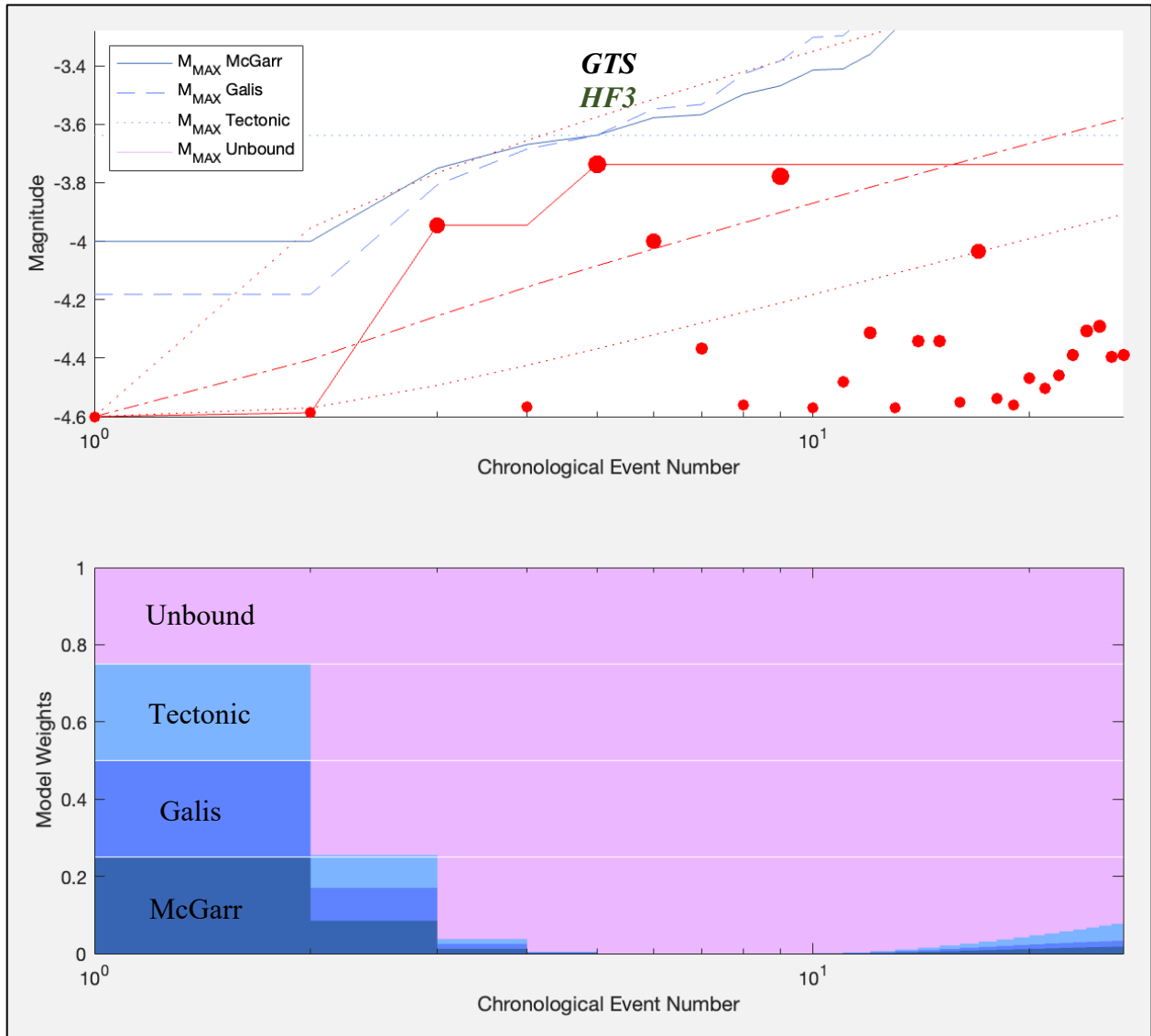
134
 135
 136
 137
 138
 139
 140
 141
 142

Figure S8. Using the EW-test to discern between M_{MAX} models for HS8 at the GTS. In the catalogue of earthquake magnitudes (red circles), the observed M_{LRG} sequence (red lines & circles), and expected M_{LRG} at the 10/50/90 percentiles (red dashed lines) are tested using three M_{MAX} assumptions (blue lines). In the bottom panel, AIC/BIC-based ensemble model weights (coloured bars) using all data prior to each new event are shown.



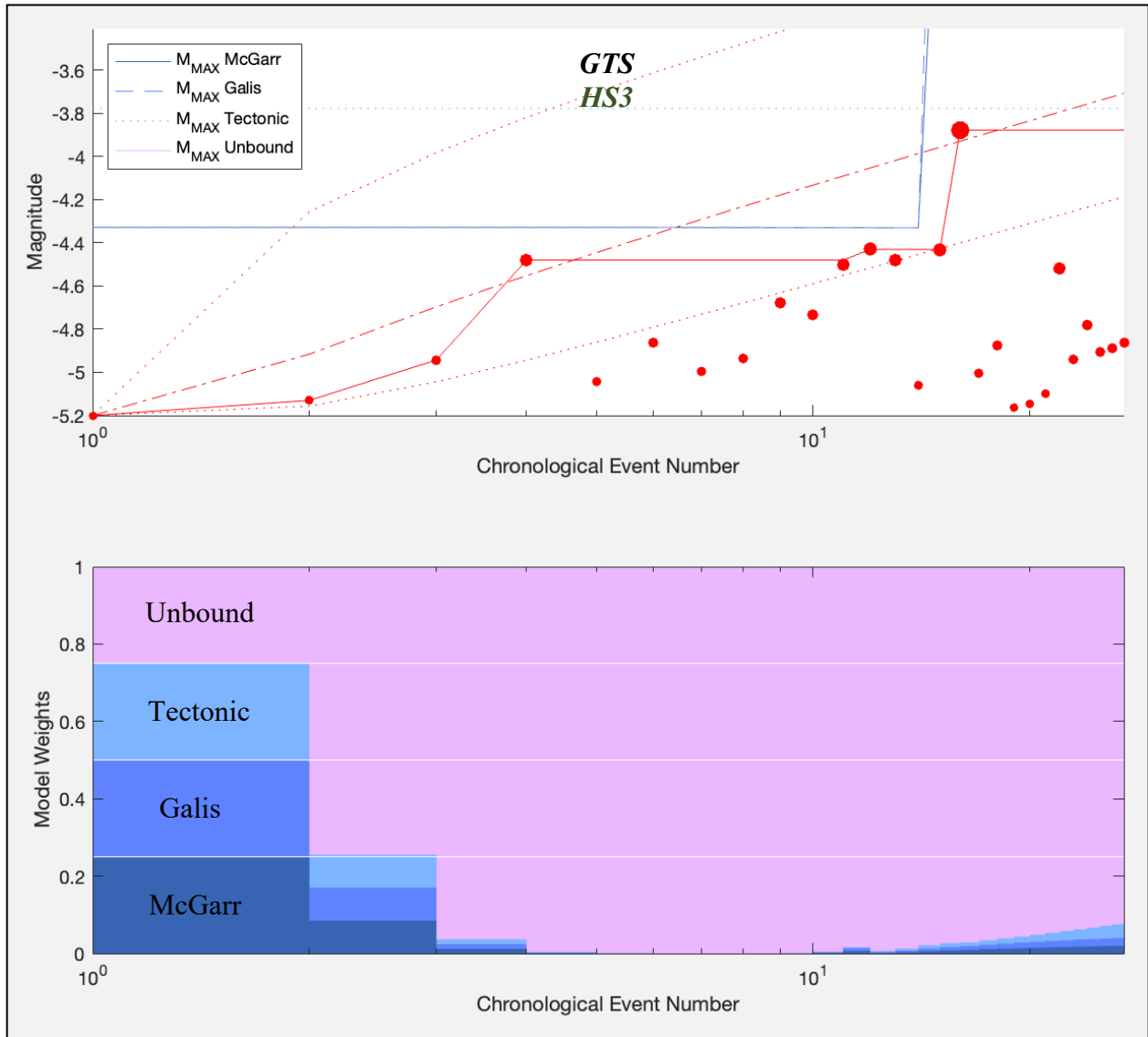
144
 145
 146
 147
 148
 149
 150
 151
 152

Figure S9. Using the EW-test to discern between M_{MAX} models for HF8 at the GTS. In the catalogue of earthquake magnitudes (red circles), the observed M_{LRG} sequence (red lines & circles), and expected M_{LRG} at the 10/50/90 percentiles (red dashed lines) are tested using three M_{MAX} assumptions (blue lines). In the bottom panel, AIC/BIC-based ensemble model weights (coloured bars) using all data prior to each new event are shown.



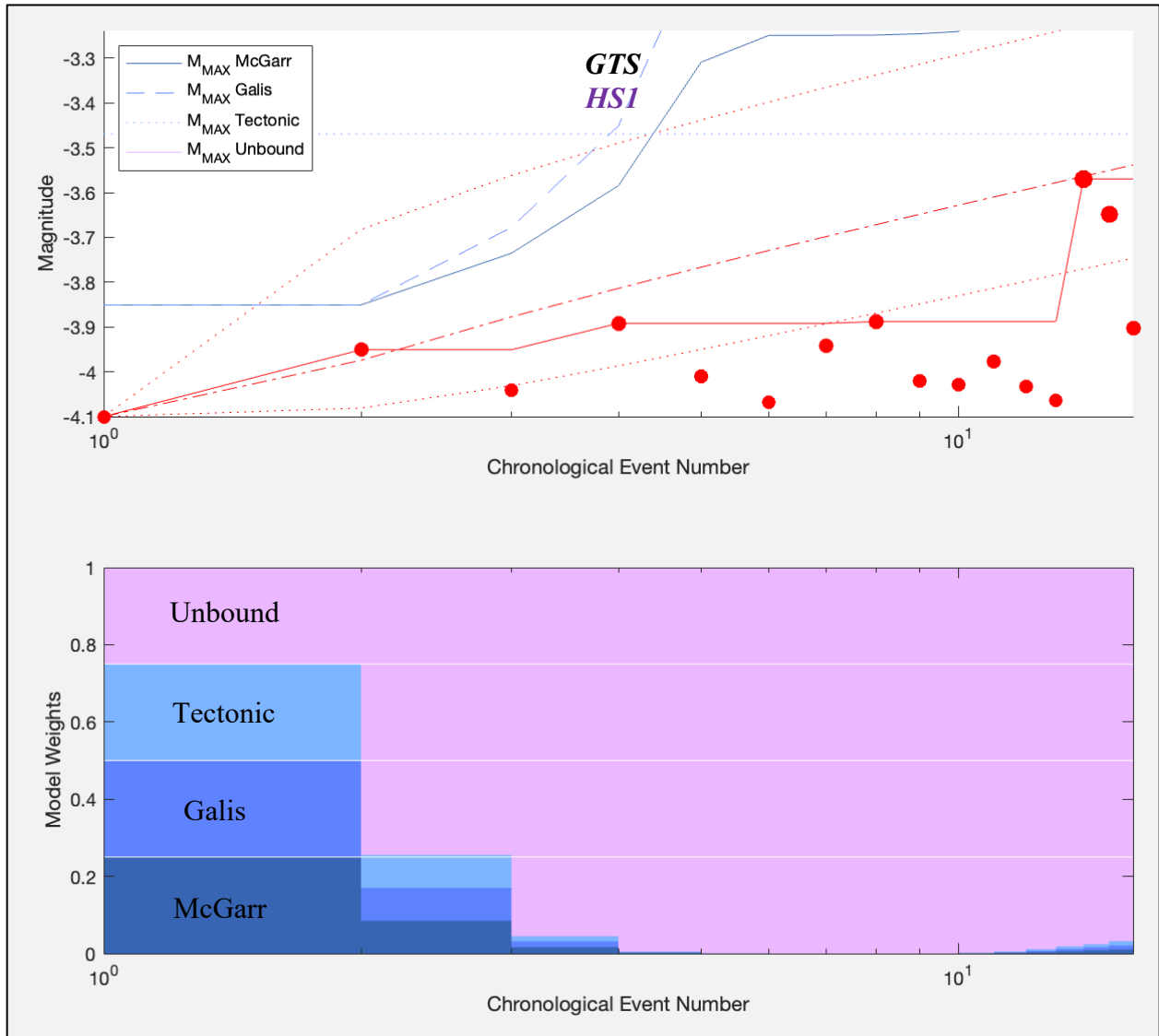
154
 155
 156
 157
 158
 159
 160
 161
 162

Figure S10. Using the EW-test to discern between M_{MAX} models for HF3 at the GTS. In the top panel, the catalogue of earthquake magnitudes (red circles), the observed M_{LRG} sequence (red lines & circles), and expected M_{LRG} at the 10/50/90 percentiles (red dashed lines) are tested using three M_{MAX} assumptions (blue lines). In the bottom panel, AIC/BIC-based ensemble model weights (coloured bars) using all data prior to each new event are shown.



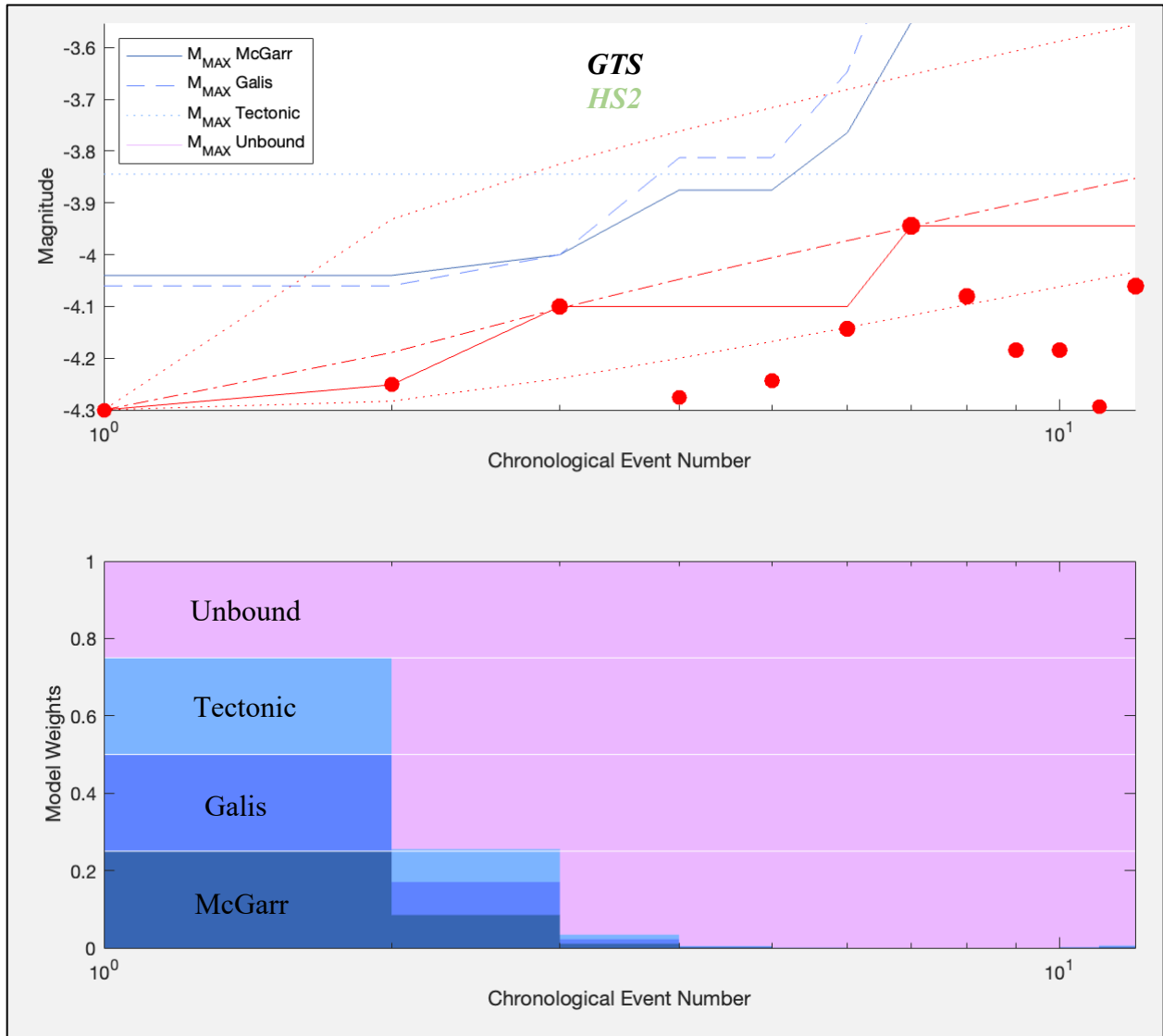
164
 165
 166
 167
 168
 169
 170
 171
 172

Figure S11. Using the EW-test to discern between M_{MAX} models for HS3 at the GTS. In the catalogue of earthquake magnitudes (red circles), the observed M_{LRG} sequence (red lines & circles), and expected M_{LRG} at the 10/50/90 percentiles (red dashed lines) are tested using three M_{MAX} assumptions (blue lines). In the bottom panel, AIC/BIC-based ensemble model weights (coloured bars) using all data prior to each new event are shown.



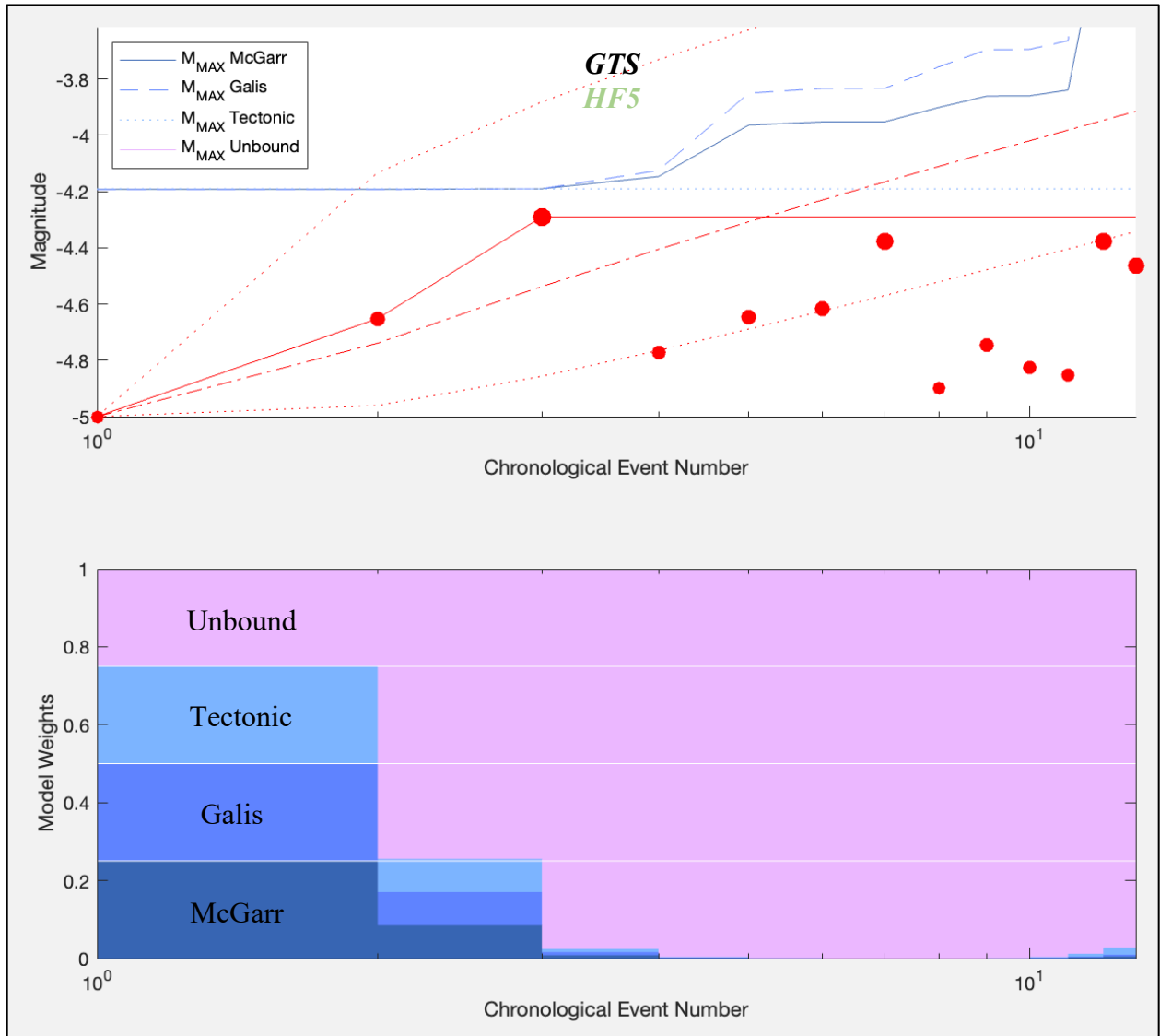
174
 175
 176
 177
 178
 179
 180
 181
 182

Figure S12. Using the EW-test to discern between M_{MAX} models for HS1 at the GTS In the catalogue of earthquake magnitudes (red circles), the observed M_{LRG} sequence (red lines & circles), and expected M_{LRG} at the 10/50/90 percentiles (red dashed lines) are tested using three M_{MAX} assumptions (blue lines). In the bottom panel, AIC/BIC-based ensemble model weights (coloured bars) using all data prior to each new event are shown.



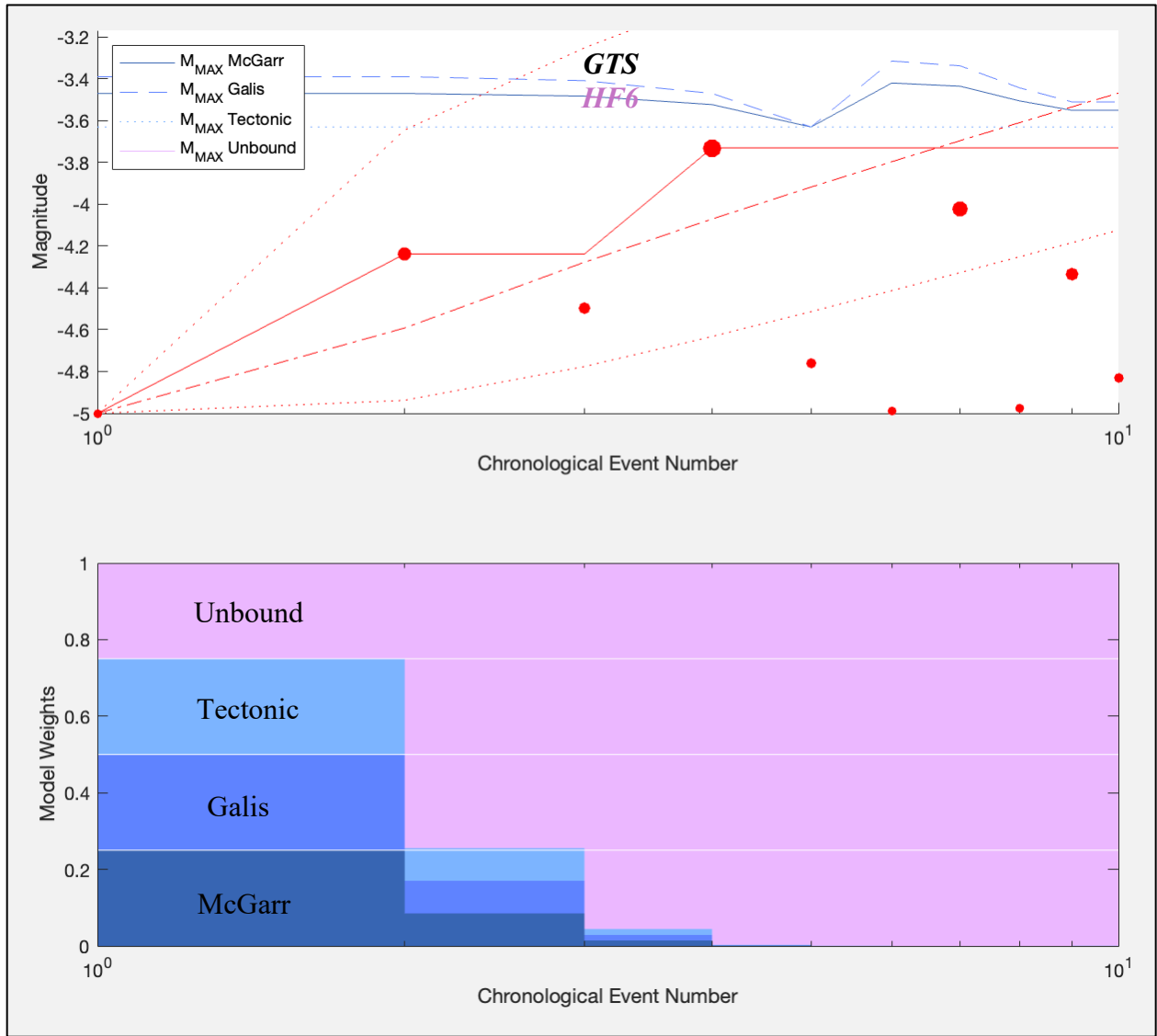
184
 185
 186
 187
 188
 189
 190
 191
 192

Figure S13. Using the EW-test to discern between M_{MAX} models for HS2 at the GTS. In the top panel, the catalogue of earthquake magnitudes (red circles), the observed M_{LRG} sequence (red lines & circles), and expected M_{LRG} at the 10/50/90 percentiles (red dashed lines) are tested using three M_{MAX} assumptions (blue lines). In the bottom panel, AIC/BIC-based ensemble model weights (coloured bars) using all data prior to each new event are shown.



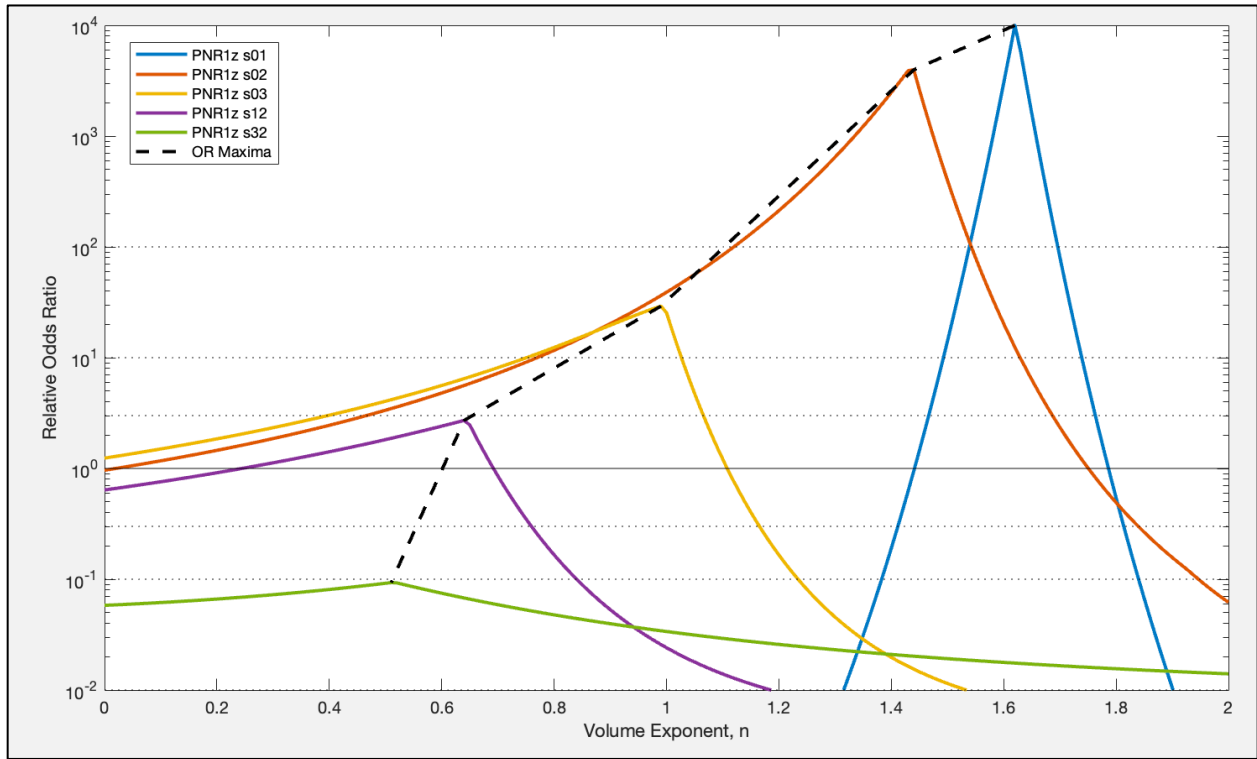
194
 195
 196
 197
 198
 199
 200
 201
 202

Figure S14. Using the EW-test to discern between M_{MAX} models for HF5 at the GTS. In the catalogue of earthquake magnitudes (red circles), the observed M_{LRG} sequence (red lines & circles), and expected M_{LRG} at the 10/50/90 percentiles (red dashed lines) are tested using three M_{MAX} assumptions (blue lines). In the bottom panel, AIC/BIC-based ensemble model weights (coloured bars) using all data prior to each new event are shown.



204
 205
 206
 207
 208
 209
 210
 211
 212

Figure S15. Using the EW-test to discern between M_{MAX} models for HF6 at the GTS. In the top panel, the catalogue of earthquake magnitudes (red circles), the observed M_{LRG} sequence (red lines & circles), and expected M_{LRG} at the 10/50/90 percentiles (red dashed lines) are tested using three M_{MAX} assumptions (blue lines). In the bottom panel, AIC/BIC-based ensemble model weights (coloured bars) using all data prior to each new event are shown.



214
 215
 216
 217
 218
 219
 220
 221
 222
 223
 224

Figure S16. Drop-out test applied to the PNR-1z data. The EW-test is repeated, with initial stages being sequentially omitted. Odds ratios of drop-out clusters (solid lines; relative to the unbound null hypothesis) are plotted alongside statistical confidence thresholds (horizontal dotted lines). The trend of relative odds ratio maxima, as a function of drop-out stages, is also highlighted (dashed black line). Note that relative odds ratios are capped at 10^4 to facilitate an easier comparison via plotting. See also Figure 14b.